Pushing the limits of magnetocaloric high-entropy alloys

Cite as: APL Mater. 9, 080702 (2021); doi: 10.1063/5.0058388
Submitted: 29 May 2021 • Accepted: 9 August 2021 •
Published Online: 23 August 2021

Jia Yan Law[a] and Victorino Franco[a]

AFFILIATIONS

Dpto. Física de la Materia Condensada, ICMS-CSIC, Universidad de Sevilla, P.O. Box 1065, 41080 Sevilla, Spain

[a]Authors to whom correspondence should be addressed: jylaw@us.es and vfranco@us.es

ABSTRACT

High-entropy alloys (HEAs) have become a topic of high research interest due to the excellent mechanical properties that can be found in this new type of materials. However, their functional properties are usually modest when compared to conventional materials. The discovery of high-entropy alloys with an optimal combination of mechanical and functional properties would be a leap forward in the reliability of devices that use them as functional elements. This Research Update focuses on magnetocaloric HEAs, showing that a directed search strategy allows us to improve their performance in a significant way, closing the pre-existing gap between magnetocaloric HEAs and high-performance magnetocaloric materials. Further challenges that remain in this line of research are highlighted.

I. INTRODUCTION

Metallurgy is circa five millennia old, and for the vast majority of its past, it has mainly focused on designing new alloys by adding minor amounts of elements to one or two main constituents. Over time, the possibilities of finding new element combinations that cause a significant enhancement of the materials' properties are getting exhausted, which motivates the search for radically new approaches for alloy development. This change of philosophy arrived with the concept of high-entropy alloys (HEAs), which utilize multiple principal elements (five or more) in relatively high concentrations to form materials with a high entropy of mixing (ΔS_{mix}). HEAs encompass a vast compositional space, which provides a large window of promising opportunities for discovery of new alloys with valuable properties. In general, there are two widely accepted ways of defining HEAs based on the configurational entropy and composition requirements.[1,2]

A. Entropy-based definition

HEAs are defined as alloys with five or more principal elements, exhibiting $\Delta S_{mix} \geq 1.5R$ regardless of being single or multiphase at room temperature, in which ΔS_{mix} is calculated as

$$\Delta S_{mix} = -R \sum x_i \ln x_i, \quad (1)$$

where R is the gas constant and x_i is the mole fraction of the ith element. It is worth noting that the entropy of mixing is usually simplified to exclusively consider the configurational entropy since this term dominates over the other contributions to the total entropy of mixing, which are vibrational, magnetic dipole, and electronic randomness. Figure 1 shows the various classifications of materials based on their configurational entropy values and number of principal elements, where the community preferentially considered that ΔS_{mix} of $1.5R$ is large enough to be used as the boundary between HEAs and medium-entropy alloys.

B. Composition-based definition

An alternate definition, based on the concentration of the different elements, can be summarized as

$$n_{major} \geq 5,\ 5\ \text{at.}\ \% \leq c_i \leq 35\ \text{at.}\ \%,$$
$$n_{minor} \geq 0,\ c_j \leq 5\ \text{at.}\ \%,$$

where n_{major} and n_{minor} represent the number of major and minor elements, respectively. Minor elements here refer to elemental additives that are usually added to HEA systems for further tuning desired properties. c_i and c_j are the atomic percentage of ith major and jth minor elements, respectively.

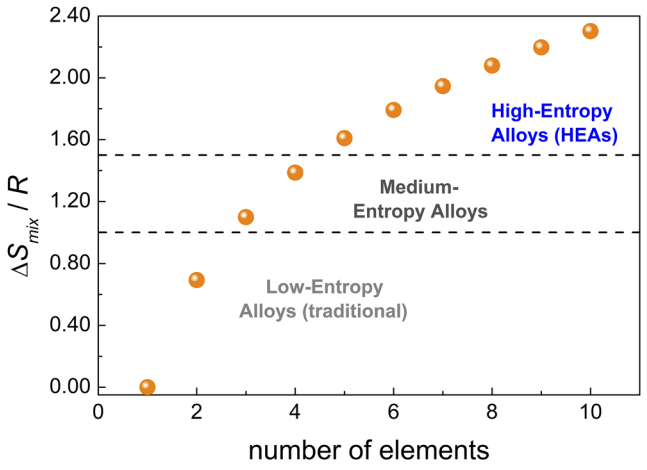

FIG. 1. Influence of the number of elements on ΔS_{mix} for equiatomic alloy systems.

In addition to the vast HEA compositional space of opportunities, HEAs have been highly regarded as a game-changer for designing new advanced materials as they have been found demonstrating remarkable mechanical properties, phase stability, wear and corrosion resistance, etc., when compared to conventional alloys.[1,2] Motivated by these advantages, the HEA research topic gains much attention and popularity, evolving to more than 5000 papers since its first publication in 2004 (based on Scopus search using "high-entropy *" in the article title). The fast extension of HEA research advances the evolution of two HEA generations from first generation equiatomic single-phase HEAs to a more recent emphasis on a second generation, with multiple or complex phases and/or non-equiatomic compositions, both covering a broad range of composition. The radar chart in Fig. 2 shows the number of publications on the various research focus of HEAs, where it is evident that most studies focus on structural (black labels) rather than functional properties (color labels). The scarcity of reports on functional HEAs is, therefore, a potential research direction. From the functional point of view, Fig. 2 evidences that the largest number of publications on functional HEAs focus on their magnetic properties, being justified by the fact that HEA compositions typically contain ferromagnetic elements, such as Fe, Co, and Ni, further alloyed with Al, Cr, and Ti for optimization of their mechanical behavior.[3,4] Next in the order of popular functional HEA studies is the magnetocaloric effect (MCE), which corresponds to the isothermal entropy change and/or adiabatic temperature change of a magnetic material induced by an applied varying magnetic field. This effect is the basis of the energy-efficient and environmental friendly magnetic refrigeration.[5] As HEAs exhibit great potential for optimal mechanical properties, they can rectify the limited mechanical integrity of most high-performance conventional magnetocaloric materials during cycling,[5] making HEAs a new class of magnetocaloric materials. However, the goal of achieving an optimal combination of mechanical and magnetocaloric properties met severe limitations, as reported MCE values of HEAs were modest and very far from being competitive when compared to high-performance conventional magnetocaloric materials, especially for rare-earth (RE) free HEAs. Only recently, HEAs undergoing magneto-structural transformations were reported,[6,7] which constitutes a significant leap for the achievement of high-performance MCE-HEAs.

While there have been many recently published review papers on HEAs, their discussions mainly centered on their mechanical properties, phase formation, and microstructure, highlighting the scarcity of functional reports. Very few of these publications are

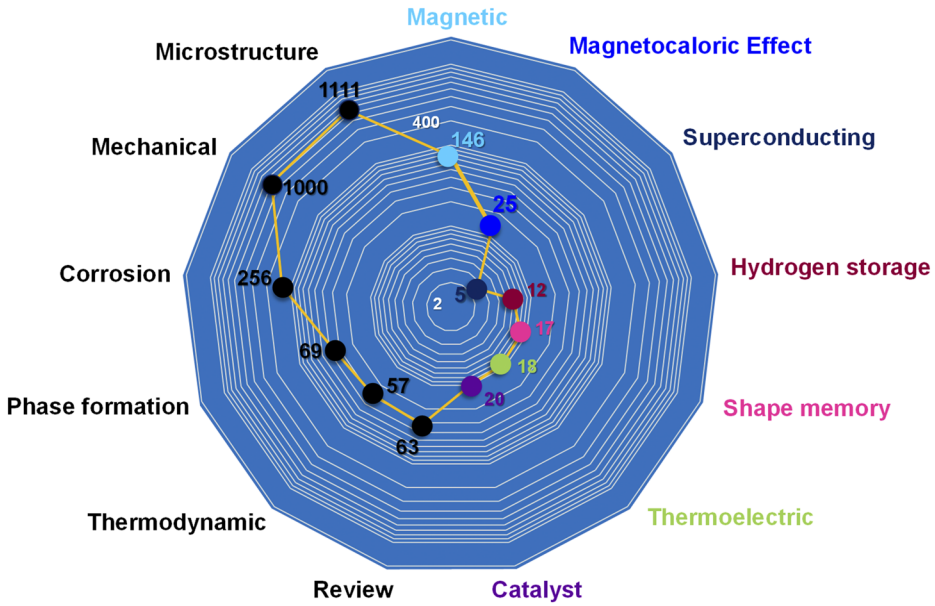

FIG. 2. The number of HEA publications and their different focus (mechanical properties, microstructure, etc.) presented in a radar chart in log scale. Bibliographic Scopus search was restricted to article titles containing "high-entropy *" plus the above-presented labels (dated up to May 2021). Reports related to functional properties are with colored labels.

dedicated to reviewing the state-of-the-art functional HEAs except for one on the mechanical and magnetic properties of HEAs[8] and another on the progress of HEAs for catalytic applications.[9] A recent book chapter reporting the MCE of HEAs has been published, which is fully dedicated on transition metal HEAs (TM-HEAs), explaining how the role of distributed exchange interactions influences the smeared magnetic behavior and thus MCE.[10] Despite the limited literature, the discovery of HEAs with an optimal combination of mechanical and functional properties will pave the path toward enhanced service life of the devices that use them, also facilitating a more circular economy.

This current Review focuses on the state-of-the-art of magnetocaloric HEAs, highlighting the motivation of their development and putting their performance in the context of conventional high-performance magnetocaloric materials. We will emphasize that an intentional, property-targeted alloy design approach is necessary for an efficient search in the vast HEA compositional space. In addition, we provide a supplementary material containing the different figures of merit used for MCE performance evaluation and their HEA empirical parameters of the reported magnetocaloric HEAs. They are classified under several tables according to RE-containing [quinary (Table TS1) and non-quinary (Table TS2)] and RE-free magnetocaloric HEAs [quinary (Table TS3) and non-quinary (Table TS4)].

II. SOME FUNDAMENTALS ON MAGNETOCALORIC PROPERTIES

MCE describes the reversible temperature change in a magnetic material when subjected to the adiabatic application of a varying magnetic field. As it involves manipulating the degrees of freedom of the magnetic sub-system with the magnetic field and their coupling to the degrees of freedom associated with the structure/lattice, MCE is considered as an intrinsic phenomenon in magnetic materials. It is very common to find works determining MCE indirectly from the isothermal magnetic change that is derived from the Maxwell relation

$$\Delta S_{isothermal} = \mu_0 \int_{H_{initial}}^{H_{final}} (\partial M/\partial T) dH, \tag{2}$$

where M, H, T, and μ_0 refer to magnetization, magnetic field, temperature, and permeability of vacuum, respectively. Other figures of merit used for comparison among magnetocaloric materials, including HEAs, include refrigerant capacity (RC), relative cooling power (RCP), and temperature averaged entropy change (TEC). In this Research Update, we select RCP, TEC, and peak values of $\Delta S_{isothermal}$ ($\Delta S^{peak}_{isothermal}$) for the performance comparison of magnetocaloric HEAs. They are calculated using the following equations:

$$RCP = \Delta S^{peak}_{isothermal} \delta_{FWHM}, \tag{3}$$

$$TEC(10) = \frac{1}{10} \max\left(\int_{T-5}^{T+5} \Delta S_{iso}(T') dT' \right) \approx \frac{\Delta S_{isothermal}(T_{peak} - 5) + \Delta S_{isothermal}(T_{peak}) + \Delta S_{isothermal}(T_{peak} + 5)}{3}, \tag{4}$$

where δ_{FWHM} corresponds to the full width at half maximum of the peak. $TEC(10)$ refers to the maximum average of the $\Delta S_{isothermal}$ over a 10 K temperature span, which can be approximated as indicated in Eq. (4) in the case that the data for the whole curve are not available, where T_{peak} is the temperature corresponding to $\Delta S^{pk}_{isothermal}$. It has been reported that this simplification is in good agreement with calculated values.[11] For further details related to the thermodynamics of MCE, it is recommended to refer to the comprehensive reviews and books on magnetocalorics.[5,12]

From the point of view of applications, the working temperature of the device should be in the proximity of the temperature of the phase transition that causes a relevant change in magnetization. Therefore, we can separate room-temperature applications, for which transition metal based materials are preferred, and cryogenic applications, for which rare-earths play a leading role. While there has been significant effort on room-temperature applications in the recent past, the expansion in the use of liquefied gas, such as hydrogen, and the energy efficiency of MCE-based gas liquefaction have expanded the interest of low-temperature magnetocaloric materials.

III. TRADITIONAL APPROACH IN MAGNETOCALORIC HEA

Magnetocaloric HEA compositions follow the same evolution from first to second HEA generation. They started from equiatomic compositions,[13–15] until some recent works' report on compositions related to the second generation of HEAs.[6,7,11,16,17] Most of the published results mainly focus on the tunability of the transition temperature, including the exploitation of distributed exchange considering the d-orbital overlap, rather than the magnitude of the magnetocaloric response, which remains considerably lower than that of conventional materials.[14,18–21]

A. Bulk amorphous HEA

Magnetocaloric HEAs began with high-entropy bulk metallic glass (HE-BMG), motivated by the strong chemical and topological disorder in HE-BMGs.[15] The community believes that such alloys may exhibit unique mechanical and physical properties that typical BMG or HEAs do not possess. As an example, $Sr_{20}Ca_{20}Yb_{20}(Li_{0.55}Mg_{0.45})_{20}Zn_{20}$ HE-BMG showed an exceptional homogeneous plastic deformation at room temperature in the absence of shear bands, which is not typical for conventional BMGs[22] (for additional examples of the unique properties of HE-BMGs, the reader is referred to Ref. 22). Hence, the first magnetocaloric HE-BMG series was $Gd_{20}Tb_{20}Dy_{20}Al_{20}M_{20}$ (M = Co, Ni, or Fe).[15] These alloys showed much larger δT_{FWHM} values compared to many RE-based BMGs, while their $\Delta S_{isothermal}$ peak values were just comparable: $\left|\Delta S^{peak}_{isothermal}\right|$ = 5.96, 7.25, and 9.43 J kg^{-1} K^{-1} (for a field of 5 T) with Curie temperatures (T_C) of 58, 45, and 112 K for M = Co, Ni, Fe, respectively. The authors then designed alloys based on

conventional RE-based BMG compositions: $R_{20}Ho_{20}Er_{20}Co_{20}Al_{20}$ (where R = Gd, Dy, or Tm).[23] They found that the alloys were fully amorphous and showed $|\Delta S_{isothermal}|$ = 11.2, 12.6, and 15.0 J kg^{-1} K^{-1} (for 5 T) with T_C = 37, 18, and 9 K for R = Gd, Dy, and Tm, respectively. These magnetocaloric properties were larger than their previous findings, though at a lower temperature range. For both works, the authors reported that the HE-BMGs underwent a second-order thermomagnetic phase transition (SOPT) based on the results from magnetic field dependence for $\left|\Delta S^{peak}_{isothermal}\right|$ and Arrott plots. More magnetocaloric investigations on bulk amorphous HEAs followed, which are briefly summarized in Fig. 3 as a flowchart to illustrate an overview of their interconnections. They are first categorized by equiatomic (EA) vs non-equiatomic compositions and the number of principal elements exhibited (quinary, quaternary, or denary), followed by the compositions that evolved from the earlier reports.

Instead of substituting rare-earths, Sheng *et al.* studied the alteration of the transition metal (TM) element in $Gd_{20}Ho_{20}Er_{20}M_{20}Al_{20}$ (where M = Co, Ni, or Fe) and further processed them into amorphous microwires (diameter of ~60 μm).[19] The authors reported T_C = 39, 25, and 55 K for M = Co, Ni, and Fe, respectively, whereby the broadest thermomagnetic curves were observed for the latter. Their maximum $|\Delta S_{isothermal}|$ values found were 10.2, 9.5, and 5.1 J kg^{-1} K^{-1} (5 T) for M = Co, Ni, and Fe, respectively. Their SOPT character was supported by the positive slopes of their Arrott plots and their power law dependence of the magnetic field dependence of $\left|\Delta S^{peak}_{isothermal}\right|$ and *RCP* values, following the criteria presented in Ref. 24.

Li *et al.* reported another magnetocaloric $Gd_{20}Ho_{20}Er_{20}Co_{20}Cu_{20}$ HEA[20] whose composition somehow resembles the formerly discussed work of Ref. 19 wherein M = Co shows the largest MCE value among $Gd_{20}Ho_{20}Er_{20}M_{20}Al_{20}$ HEA series. Hence, we have connected these works in Fig. 3 although not explicitly indicated in the report. Amorphous $Gd_{20}Ho_{20}Er_{20}Co_{20}Cu_{20}$ was melt-spun into 25–35 μm thick ribbons, which displayed itself undergoing a broad ferromagnetic to paramagnetic (FM-PM) phase transition at T_C ~ 49 K. This led to a broad $|\Delta S_{isothermal}|$ behavior (maximum value = 11.1 J kg^{-1} K^{-1} for 5 T), described by the authors as a table-like MCE (i.e., constant $|\Delta S_{isothermal}|$ over a broad temperature span near T_C). Table-like MCE was also reported for equiatomic $Gd_{20}Ho_{20}Tm_{20}Ni_{20}Cu_{20}$ amorphous ribbons,[25] which fulfill the HEA definition, with maximum $|\Delta S_{isothermal}|$ = 10.6 J kg^{-1} K^{-1} (5 T) and T_C = 32 K. The authors reported that it undergoes a SOPT and investigated the temperature averaged entropy change over a temperature span of 10 K [*TEC*(10)] and reported values of 10.52 J kg^{-1} K^{-1} (for 5 T). Equiatomic $Er_{20}Ho_{20}Tm_{20}Cu_{20}Co_{20}$ amorphous ribbons reported by Dong *et al.*[26] also fulfill the HEA definition. They exhibited $\left|\Delta S^{peak}_{isothermal}\right|$ value of 15.73 J kg^{-1} K^{-1} (5 T) with T_C of ~13.5 K. The SOPT nature of this alloy was demonstrated by the collapse of the different $|\Delta S_{isothermal}(T)|$ curves onto a single universal curve.

An extended investigation, also motivated by the RE-BMG compositions, reported magnetocaloric $R_{20}Dy_{20}Er_{20}Co_{20}Al_{20}$ (where R = Gd, Tb, or Tm) HE-BMGs.[27] The maximum $|\Delta S_{isothermal}|$ values found are 9.1, 8.6, and 11.9 J kg^{-1} K^{-1} (for 5 T) with T_C = 43, 29, and 13 K for R = Gd, Tb, and Tm, respectively. They were also found to undergo SOPT and had broad δT_{FWHM}, which then led to large *RCP* values similar to other magnetocaloric RE-HEAs. A recent publication on amorphous ribbons of $Gd_{20}Tm_{20}Er_{20}Co_{20}Al_{20}$ HEA reports a power law correlation between MCE and magnetoresistance.[28] The authors also attributed their observed difference between the MCE values obtained for perpendicular and parallel fields to the role of magnetic anisotropy associated with that of atomic packing. The largest $\left|\Delta S^{pk}_{isothermal}\right|$ value reported in the work (5 T) is 9.7 J kg^{-1} K^{-1}, which is comparable to that of the $Gd_{20}Dy_{20}Er_{20}Co_{20}Al_{20}$ HEA[27] despite at a lower T_C (32.1 vs 43 K for $Gd_{20}Tm_{20}Er_{20}Co_{20}Al_{20}$ and $Gd_{20}Dy_{20}Er_{20}Co_{20}Al_{20}$, respectively).

Aside from the above-mentioned quinary equiatomic HE-BMGs, there were also works on quaternary equiatomic magnetocaloric HE-BMGs. Xue *et al.* investigated the effect of different

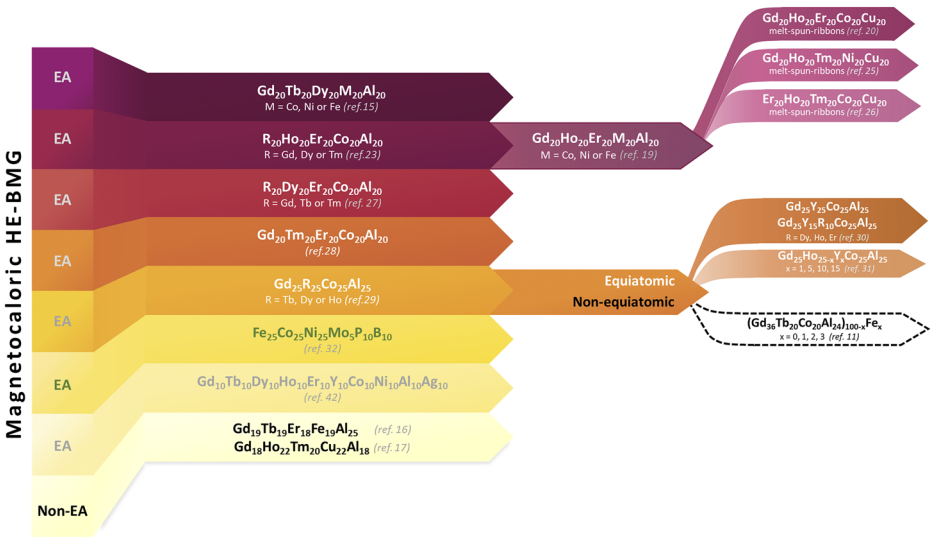

FIG. 3. A flowchart depicting the relevance to the works reported on bulk amorphous HEAs for magnetocaloric investigations as an overview. The elemental sequence is rearranged from the literature to help the readers correlate the different works. EA refers to equiatomic compositions.

RE elements in $Gd_{25}R_{25}Co_{25}Al_{25}$ HEAs (R = Tb, Dy, or Ho) and reported that these amorphous ribbons showed $|\Delta S^{peak}_{isothermal}|$ = 8.88, 8.72, and 9.78 J kg^{-1} K^{-1} (for 5 T) at T_C = 73, 60, and 50 K for R = Tb, Dy, and Ho, respectively.[29] Their magnetic field dependence of $|\Delta S^{peak}_{isothermal}|$ values follows a power law expression, which indicated that these alloys underwent a SOPT. Pang *et al.* reported the MCE of $Gd_{25}Y_{25}Co_{25}Al_{25}$ and $Gd_{25}Y_{15}R_{10}Co_{25}Al_{25}$ (R = Dy, Ho, or Er) high-entropy metallic glasses (HE-MGs)[30] and found that the latter exhibited $|\Delta S^{peak}_{isothermal}|$ = 6.02 J kg^{-1} K^{-1} (5 T) at T_C = 39 K. For R = Dy, Ho, and Er of the alloy series, $|\Delta S^{peak}_{isothermal}|$ = 6.76, 7.35, and 6.96 J kg^{-1} K^{-1} (5 T) at T_C = 44, 41, and 43 K, respectively. These four HEAs were also found exhibiting amorphous structure and undergoing a SOPT. As the substitution of Y by adjacent heavy RE elements in $Gd_{25}Y_{15}R_{10}Co_{25}Al_{25}$ showed MCE improvement (especially for R = Ho, whose $|\Delta S^{peak}_{isothermal}|$ was the largest among others), Pang *et al.* followed up on another systematic study on the influence of Y on the magnetocaloric properties of amorphous $Gd_{25}Ho_{25-x}Y_xCo_{25}Al_{25}$ (x = 1, 5, 10, and 15) for further optimization.[31] The ribbons displayed $|\Delta S^{peak}_{isothermal}|$ = 8.63, 8.79, 7.61, and 7.35 J kg^{-1} K^{-1} (5 T) at T_C = 51, 49, 47, and 41 K for x = 1, 5, 10, and 15, respectively. Among the series, it is observed that $|\Delta S^{peak}_{isothermal}|$ decreases for x = 10 and 15, which the authors attribute to the reduction in magnetic interactions between RE elements due to the negligible Y moment. For x = 1 and 5, the latter exhibits a larger $|\Delta S^{peak}_{isothermal}|$ value, which the authors attribute to the complex spatial inhomogeneity of Y-containing metallic glasses corresponding to the increase in ΔS_{mix}. The SOPT character of these HE-MGs was supported by the Arrott plot analysis as well as the power-law relationship for the magnetic field dependence of magnetocaloric parameters.

There is also a related work investigating magnetocaloric RE-free HE-BMG: $Fe_{25}Co_{25}Ni_{25}Mo_5P_{10}B_{10}$[32] (labeled with green font color in Fig. 3). It exhibited a wide δT_{FWHM} with $|\Delta S^{peak}_{isothermal}|$ = 0.8 (1.5 T) and 1.88 J kg^{-1} K^{-1} (5 T) at T_C = 560 K, where the authors indicated that these values are not better than their selected list of typical Fe-based magnetocaloric alloys,[33–37] Fe-based BMGs,[38,39] as well as the RE-containing HE-BMGs, except for Co-based metallic glasses.[40,41] The peak $|\Delta S_{isothermal}|$ values showed a linear correlation with saturation magnetization, in agreement with the behavior found for several selected transition metal (TM)-based BMGs. The authors further reported that the high-entropy effect does not contribute to the magnitude of $|\Delta S_{isothermal}|$ but widened the δT_{FWHM}, making the *RCP* values similar to the reports of RE-containing HE-BMGs.[15]

Extension of the equiatomic quinary magnetocaloric HE-BMGs was reported for equiatomic denary $Gd_{10}Tb_{10}Dy_{10}Ho_{10}Er_{10}Y_{10}Ni_{10}Co_{10}Ag_{10}Al_{10}$ HE-MG ribbons.[42] Their T_C is 24 K with a peak $|\Delta S_{isothermal}|$ value of 10.64 J kg^{-1} K^{-1} (5 T). The magnetic field dependence of $|\Delta S^{peak}_{isothermal}|$ and *RCP* follow a power law expression, indicating the SOPT nature of the alloy. When compared to other magnetocaloric RE-HEAs and conventional RE-based BMGs, the authors reported that the magnetocaloric properties of the denary HE-MG were not unexpected, indicating no distinct cocktail effect (one of the phenomena leading to unexpected properties of HEAs).

The second HEA generation with compositions deviating from equiatomic compositions (labeled with black font color in Fig. 3) can be found in the recent work of Luo *et al.*, in which high-entropy $Gd_{19}Tb_{19}Er_{18}Fe_{19}Al_{25}$ amorphous microwires were developed and studied for their MCE.[16] The alloy showed a maximum $|\Delta S_{isothermal}|$ of ~ 5.94 J kg^{-1} K^{-1} (5 T) with T_C = 97 K. Its SOPT-nature was supported by the positive slopes observed in its Arrott plots, according to Banerjee's criterion. Another non-equiatomic bulk amorphous HEA studied for its MCE was $Gd_{18}Ho_{22}Tm_{20}Cu_{22}Al_{18}$, recently reported by Dong *et al.*[17] The amorphous ribbons exhibited an $|\Delta S^{pk}_{isothermal}|$ value of 8.70 J kg^{-1} K^{-1} (5 T), with a SOPT-nature and T_C of ~ 33.6 K. The authors also reported its universal curve behavior and *TEC*(10) values (8.55 J kg^{-1} K^{-1} for 5 T). Very recently, minor Fe doping to non-equiatomic $(Gd_{36}Tb_{20}Co_{20}Al_{24})_{100-x}Fe_x$ HE-MGs (drawn as a dashed line in Fig. 3) was reported to optimize MCE up to 108 K.[11] The microwires exhibit a dual amorphous-nanocrystalline microstructure as x increases to 2 and 3, which contributes to the broadening of the δT_{FWHM} and thus the increase in the *RC* and *RCP* values.

B. Crystalline RE-containing HEA

Section III A on amorphous magnetocaloric HEAs showed that most of the work was centered on RE-containing compositions, probably due to the good intrinsic magnetic properties exhibited by RE elements. Although RE-containing magnetocaloric HEAs are mainly amorphous, the crystalline $Gd_{20}Tb_{20}Dy_{20}Ho_{20}Er_{20}$ HEA[43] draws the most attention in the HEA community and it is usually cited in review papers when promoting HEAs for magnetic refrigeration applications. Its empirical parameters for HEA design fall in the range of a single-phase solid solution. It exhibits refrigerant capacity values larger than many other magnetic refrigeration materials, within the same temperature range, due to the broad temperature span arising from its various types of magnetic phase transitions, antiferromagnetic to ferromagnetic (AFM-FM) followed by ferromagnetic to paramagnetic (FM-PM) up to 300 K, as confirmed by thermomagnetic and differential scanning calorimetry (DSC) results. The latter shows a broad hump at low temperatures (<150 K) and another broad λ singularity at the Néel temperature of 186 K, which indicates SOPT. This identification of the order of the phase transition is in contrast with the Arrott plots of the alloy, which show negative slopes for T < 185 K, indicating a first-order thermomagnetic phase transition (FOPT), and positive slopes for T > 185 K, indicating SOPT. However, no further discussion was provided in the publication. It has to be noted that for characterizing FOPT materials, one should utilize the discontinuous measurement protocol to erase the prior state of the sample so that no spurious MCE results will appear during analysis (refer to Ref. 44 for the protocol details). As detailed information on the procedure followed for isothermal magnetization measurements was not given, the apparently conflicting interpretation of the order of the phase transition cannot be discerned without further measurements and the use of the quantitative procedure.[45] The authors reported the $|\Delta S^{peak}_{isothermal}|$ and *RCP* values of the $Gd_{20}Tb_{20}Dy_{20}Ho_{20}Er_{20}$ HEA for 5 T as 8.6 J kg^{-1} K^{-1} and 895 J kg^{-1}. More details on these values and

other MCE figures of merit for 2 T are available in the tables in the supplementary material.

Recently, the $Gd_{20}Tb_{20}Ho_{20}Er_{20}Y_{20}$ HEA, crystallizing in hexagonal closed packed (HCP) structure, was reported to undergo AFM-FM at low temperatures (Néel temperature of 163 K) for low magnetic fields, followed by FM-PM at higher temperatures.[46] The authors reported that the negative slopes for T < 163 K in the Arrott plots indicate FOPT. All these observations are similar to those of the $Gd_{20}Tb_{20}Dy_{20}Ho_{20}Er_{20}$ HEA[43] except for the MCE behavior at fields higher than 2 T, where two direct MCE peaks are observed, ~0.25 and 1.11 J kg^{-1} K^{-1} (2 T) at ~125 and ~165 K, respectively. The authors added that the two MCE peaks lead to a broad temperature span, thus contributing to a large refrigerant capacity value, 453 J kg^{-1} for 5 T (yet 27.8% smaller than that for the $Gd_{20}Tb_{20}Dy_{20}Ho_{20}Er_{20}$ HEA). They also reported another study on the MCE of quaternary–quinary–senary RE-HEAs.[47] For $Gd_{25}Tb_{25}Ho_{25}Er_{25}$, $Gd_{20}Tb_{20}Ho_{20}Er_{20}La_{20}$ vs $Gd_{16.67}Tb_{16.67}Ho_{16.67}Er_{16.67}La_{16.67}Y_{16.67}$, $\left|\Delta S^{peak}_{isothermal}\right|$ decreases from 8.64 → 5.92 → 5.85 J kg^{-1} K^{-1} (5 T), respectively. The authors attribute the MCE reduction to the dilution of the overall magnetization of the alloys due to the non-magnetic nature of La and Y. The MCE comparison among quinary RE-HEAs include $Gd_{20}Tb_{20}Ho_{20}Er_{20}La_{20}$, $Gd_{20}Tb_{20}Dy_{20}Ho_{20}Er_{20}$, and $Gd_{20}Tb_{20}Ho_{20}Er_{20}Pr_{20}$, where La is the only non-magnetic RE element, while Dy (9.72 μ_B)[48] and Pr (3.58 μ_B)[48] are magnetic. Their $\left|\Delta S^{peak}_{isothermal}\right|$ values are 5.92, 8.6, and 6.92 J kg^{-1} K^{-1} (5 T). The authors attribute that the magnetic and the magnetocaloric behavior of GdTbHoErX HEAs are dependent on the 4f electrons of the RE element (used for X) instead of ΔS_{mix}.

Figure 4 shows the $\left|\Delta S^{peak}_{isothermal}\right|$ values (for 5 T) vs transition temperatures of $Gd_{20}Tb_{20}Dy_{20}Ho_{20}Er_{20}$ HEAs in comparison with the bulk amorphous HEAs. It can be observed that only the RE-free bulk amorphous $Fe_{25}Co_{25}Ni_{25}Mo_5P_{10}B_{10}$ (green symbol)[32] exhibited the highest transition temperature, while the other bulk amorphous HEAs (containing RE; open and closed symbols) are saturated around the low temperature region, T < 150 K. However, the $\left|\Delta S^{peak}_{isothermal}\right|$ for the RE-free alloy is the lowest when compared to all other RE-containing magnetocaloric HEAs. The well-received $Gd_{20}Tb_{20}Dy_{20}Ho_{20}Er_{20}$ HEA, composed only of RE elements, is located above this low temperature region at 186 K. Although there are several RE-containing bulk amorphous HEAs exhibiting larger $\left|\Delta S^{peak}_{isothermal}\right|$ than $Gd_{20}Tb_{20}Dy_{20}Ho_{20}Er_{20}$ HEAs, their transition temperatures mainly centered below 60 K and only a few can be found around 60–110 K.

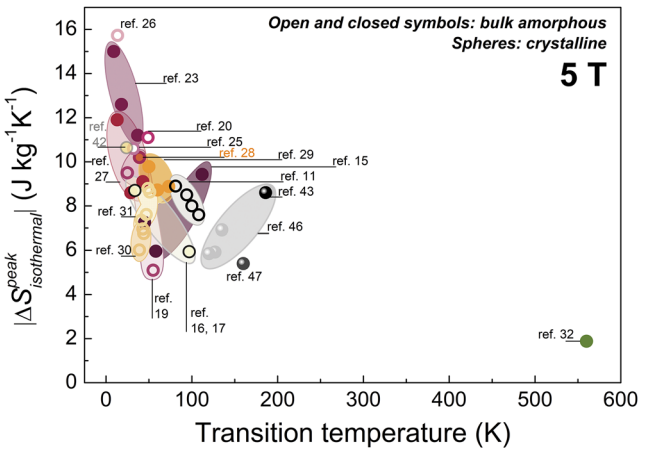

FIG. 4. MCE performance comparison of bulk amorphous (open and closed symbols) and crystalline HEAs (spheres) vs the notable Gd_{20} Tb_{20} Dy_{20} $Ho_{20}Er_{20}$ crystalline HEAs (black sphere with text label, "Ref. 43").

C. Transition metal HEA

For the RE-free magnetocaloric HEAs, they usually comprise TM elements, for which initial investigations mainly focused on tuning their transition temperatures. The work of Lucas *et al.* on the enhancement of magnetic properties and T_C of FeCoNiCr-type HEAs via Pd alloying[49] showed that $FeCoNiCrPd_x$ (x = 1 to 2) had a tunable T_C of 440–503 K when changing the Pd content and, at the same time, improved the saturation magnetization (M_S) with Pd addition. They also reported a thermomagnetic study of another series of $FeCoNiCr_x$ HEAs (x = 0.5–1.15), in which T_{peak} values decrease with higher Cr content due to the reduced average exchange interaction.[13] Their reported MCE values were below 0.4 J kg^{-1} K^{-1} (2 T) for cold-rolled states and after heat treatment, finding that their magnitudes are about one quarter the MCE of γ-$Fe_{70}Ni_{30}$.[50] Further analysis of the thermomagnetic curves of cold-rolled vs heating from the as-rolled state shows a re-entrant magnetic moment due to a second magnetic phase upon heating, in agreement with the changes in the diffraction pattern and magnetocaloric properties. The authors suggested that such observations might arise from the changes in short range order or the merging of vacancies forming stacking faults. Subsequently, $FeCoNiCrPd_x$[14] with x = 0–0.50 SOPT HEAs were found exhibiting a tunable range of transition temperatures from ~100 to 300 K in as-rolled and annealed states, while their $\left|\Delta S^{peak}_{isothermal}\right|$ values remained below 1 J kg^{-1} K^{-1} (for 5 T). A flowchart illustrating the interconnections of the different reported RE-free magnetocaloric HEAs is briefly summarized in Fig. 5, where those only studied for their tunable T_C are further indicated with the label "T_C only," and those with MCE studies are labeled "MCE."

Later, Na *et al.* reported on alloying Mn, Al, Ga, and Sn to FeCoNiCr HEAs and produced equiatomic FeCoNiCrM (M = Mn, Al, Ga, or Sn) HEAs.[51] While FeCoCrNiMn showed a single FCC phase similar to that of FeCoCrNi, dendritic microstructures composed of BCC-matrix (Ni- and Ga-enriched) and FCC-island (Fe-, Co-, and Cr-dominant) phases were observed for FeCoNiCrAl and FeCoNiCrGa HEAs. Only the additions of Al and Ga to FeCoNiCr changed the parent PM behavior at room temperature to FM. It is interesting to note that equiatomic FeCoNi is FM with M_S = 161 A m^2 kg^{-1} but changed to PM at room temperature for equiatomic FeCoNiCr. Although the decrease in M_S of FeCoNiCrAl (25 A m^2 kg^{-1}) and FeCoNiCrGa (38 A m^2 kg^{-1}) HEAs is likely due to the dilution effects when alloyed with non-magnetic Al and Ga, their T_C could be tuned from 104 K (FeCoNiCr) to

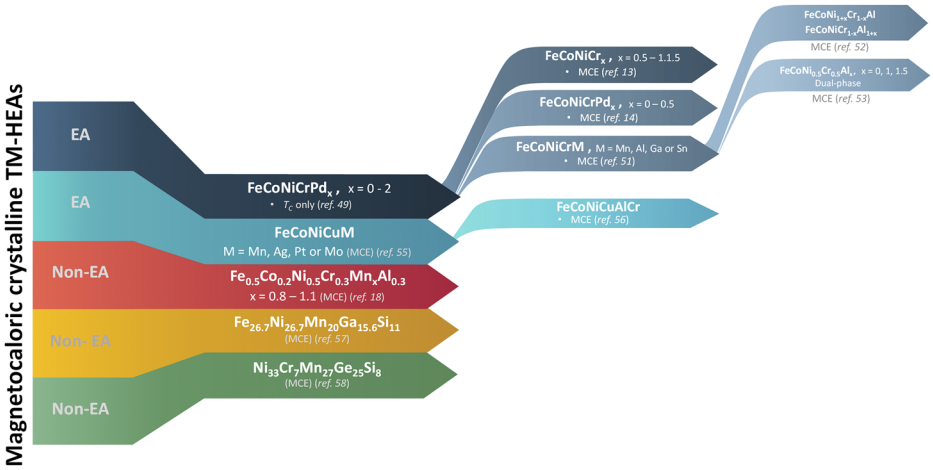

FIG. 5. A flowchart depicting the relevance to the works reported on RE-free magnetocaloric HEAs. The elemental sequence is rearranged from the literature as a guide to the readers for correlating the different works.

277 and 703 K, respectively. The authors later extended this work to a systematic compositional variation study to further tune T_C in $FeCoNi_{1+x}Cr_{1-x}Al$ and $FeCoNiCr_{1-x}Al_{1+x}$ (for both cases x = 0–0.5) HEAs[52] based on equiatomic FeCoNiCrAl. They found that FeCoNiCrAl and $FeCoNi_{1.5}Cr_{0.5}Al$ HEAs displayed very broad magnetic phase transitions from 100 to 350 K with $|\Delta S_{isothermal}|$ values of 0.674 (for 7 T at 290 K) and 0.277 J kg^{-1} K^{-1} (for 2 T at 150 K), respectively. A recent study on $FeCoNi_{0.5}Cr_{0.5}Al_x$ HEAs reported that the alloys exhibited $|\Delta S_{isothermal}|$ values of 0.56, 0.40, and 0.50 J kg^{-1} K^{-1} (2 T) for x = 0, 1, and 1.5, respectively.[53] These HEAs showed a dual phase of Fe–Cr-rich nanoparticles segregated within an AlNiCo-rich matrix, supported by their x-ray diffraction, microstructural, and thermomagnetic results. The authors further showed the dual phase behavior using the universal curve method,[24] which could enable the phase deconvolution of multiphase magnetocaloric materials (as reported in Ref. 54).

Kurniawan *et al.* studied FeCoNiCuM (M = Mn, Ag, Pt, or Mo) HEAs for T_C engineering, in which they found that their equiatomic alloys stabilized in the FM face-centered cubic (FCC) γ-phase (except for M = Ag and Mo), T_C ranges from 400 to above 1000 K, and slight deviations from equiatomic compositions could further tune the T_C to near room temperature.[55] The reported MCE values were below 1 J kg^{-1} K^{-1} for a small magnetic field change of 0.55 T, and no further information for predicting the MCE at higher fields was available.

Thin films of FeCoNiCuAlCr HEAs fabricated by mosaic targets in magnetron sputtering enabled stoichiometric variation when the surface area of the target segment modifies.[56] Its thermomagnetic behavior shows a broad maximum similar to those observed for superparamagnetic systems, with a blocking temperature at about 325 K. For magnetocaloric properties, the material demonstrates a similar smeared behavior to several RE-free HEAs in the literature, 0.53 (perpendicular to the field) and 0.38 J kg^{-1} K^{-1} (parallel to the field) for 5 T in a wide temperature span of ~200–325 K. Hence, the authors added that the magnetic cooling of these films would be ineffective, similar to the reports from Refs. 52 and 55.

Very recently, research on magnetocaloric TM-HEAs has deviated from the equiatomic compositions, evolving from the first to second HEA generation (see the "non-EA" categories in Fig. 5). The $Fe_{0.5}Co_{0.2}Ni_{0.5}Cr_{0.3}Mn_{0.89}Al_{0.3}$ HEA of duplex structure (BCC and FCC) was found exhibiting a round MCE peak (~0.16 J kg^{-1} K^{-1} for ~0.78 T) at ~326 K.[18] The authors calculated the magnetocaloric properties of the single BCC phase $Fe_{0.5}Co_{0.2}Ni_{0.5}Cr_{0.3}Mn_xAl_{0.3}$ (0.8 < x < 1.1) HEAs by normalizing their measured data with the BCC phase fraction obtained from XRD results and reported that single BCC phase $Fe_{0.5}Co_{0.2}Ni_{0.5}Cr_{0.3}Mn_{0.94}Al_{0.3}$ can be a promising magnetocaloric HEA within their selection for literature comparison. Thus, they added that stabilizing the BCC phase is an interesting direction for future work.

Sarlar *et al.*, with the aim of increasing magnetic properties in magnetocaloric HEAs, reported a non-equiatomic $Fe_{26.7}Ni_{26.7}Mn_{20}Ga_{15.6}Si_{11}$ alloy where the amounts of Fe and Ni were increased to more than equiatomic percent (i.e., 20 at. %) at the expense of Ga and Si.[57] They found that by annealing the pieces from an as-cast 2-mm-diameter rod could enhance the $\left|\Delta S^{peak}_{isothermal}\right|$ values from ~0.65 to 1.59 J kg^{-1} K^{-1} (both for 2 T) and T_C from 322 to 334 K, which shows promising MCE values among the magnetocaloric TM-HEAs (compared to those discussed above). The same authors also reported another RE-free magnetocaloric HEA—$Ni_{33}Cr_7Mn_{27}Ge_{25}Si_8$, retaining their former interests in strengthening the overall magnetic properties of the alloy when performing their elemental selections.[58] $Ni_{33}Cr_7Mn_{27}Ge_{25}Si_8$ exhibited an orthorhombic structure (*Pnma*, space group No. 62) at room temperature and $\left|\Delta S^{peak}_{isothermal}\right|$ = 2.49 J kg^{-1} K^{-1} (2 T) with a T_C = 412 K, which belongs to a SOPT-type. It is noteworthy to indicate that this MCE value is ~57% larger than that of $Fe_{26.7}Ni_{26.7}Mn_{20}Ga_{15.6}Si_{11}$ HEAs,[57] and both of these magnetocaloric TM-HEAs displayed higher MCE magnitudes among magnetocaloric TM-HEAs, without having to rely on the intrinsic large magnetic moments of RE elements. This suggests that non-equiatomic compositions could be interesting for further exploration for RE-free magnetocaloric HEAs as their $|\Delta S_{isothermal}|$ values doubled when compared to other equiatomic magnetocaloric RE-free HEAs during the MCE performance comparison presented in Fig. 6. However, the magnitudes of these values are still regarded as modest as compared to high-performance conventional magnetocaloric materials[5] due to the distributed exchange interactions that arise from the disorder, as pointed out by Perrin *et al.*[10,59]

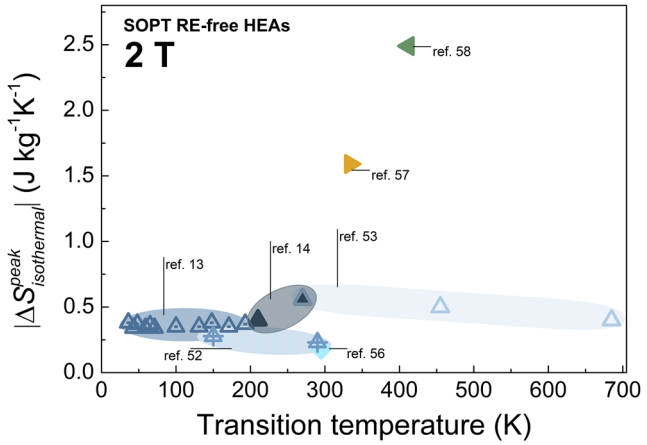

FIG. 6. MCE performance comparison of RE-free magnetocaloric HEAs for 2 T. Note that the $|\Delta S^{peak}_{isothermal}|$ values for these cases are much smaller compared to those HEAs containing RE.

IV. IMPROVED MCE HEA

A large MCE will require an abrupt change in magnetization with changing temperature, as seen from Eq. (2), which is not solely dependent on the magnitude of the magnetization of the material. HEAs are comprised of elements in high concentrations to yield large ΔS_{mix}. For magnetic systems, these large amounts of alloying elements will lead to dilution effects that broaden the transitions. This, in turn, reduces MCE. One possible solution to this complication could be to implement a magnetostructural phase transition to enhance the performance for magnetocaloric HEAs, in agreement with Ref. 60, which has proposed half-Heusler phases as the starting point to search for HEAs with improved functional properties. However, the vast HEA compositional space makes rational search challenging, making exploration strategies necessary to select starting HEAs for further optimization. Recently, Law *et al.* reported significant improvement for RE-free Fe–Mn–Ni–Ge–Si HEAs, closing the gap between high-performance conventional magnetocaloric materials and magnetocaloric HEAs[7] (see Fig. 7) via a directed search approach (further described in Sec. IV A), achieving $|\Delta S^{peak}_{isothermal}|$ values more than one order of magnitude larger than the typical values of HEAs without any RE elements. Furthermore, their magnetostructural transformations enabled them to be on par with the HEAs containing RE elements, surpassing the notable $Gd_{20}Dy_{20}Er_{20}Ho_{20}Tb_{20}$ HEA. The comparison matrix in Fig. 7 lists the largest $|\Delta S^{peak}_{isothermal}|$ for 2 T in the particular T_{peak} span for the respective family of magnetocaloric materials. Two groups of magnetocaloric materials are selected: promising conventional materials (gray text) vs HEAs (black text). Each of them is arranged in an ascending order where those with the largest MCE values are found in the middle of the chart. It can be observed that Fe–Mn–Ni–Ge–Si HEAs close the pre-existing gap between the conventional magnetocaloric materials and magnetocaloric HEAs (in red box).

A. Directed search strategy

For conventional alloys, it is possible to use brute force for optimizing binary and ternary alloy systems as the number of combinations is more manageable. However, this is not viable for systems

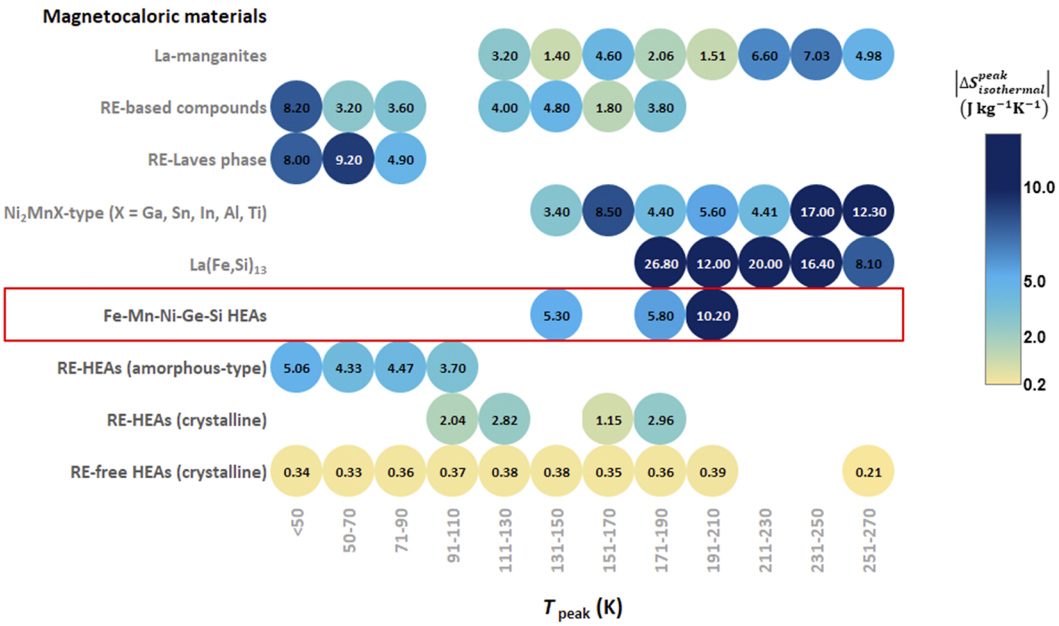

FIG. 7. MCE comparison matrix for magnetocaloric HEAs vs high-performance conventional magnetocaloric materials for 2 T. Literature data collected from Refs. 5–7, 11, 14, 23, 31, 43, 46, 47, and 62–67.

comprising five elements and above. Law *et al.* recently reported on using a property-directed search strategy to design magnetocaloric HEAs with desired behavior with the aim of improving the modest MCE values of RE-free HEAs.[6] The approach adopted was based on appropriate and intentional element substitutions to a starting composition with the desired behavior (also in line with the suggestions made in Refs. 60 and 61) and then further tuning it toward the HEA region.

The initial composition selected is based on the following considerations:

(i) starting composition should display the desired behavior,
(ii) the doping element(s) ought to be chemically compatible for isostructural substitutions, and
(iii) the elemental stoichiometry (including the substitutions) should be maintained.

B. The Fe–Ni–Mn–Ge–Si HEA case

As large magnetocaloric response is usually associated with a magnetostructural transformation, the initial composition in Refs. 6 and 7 was selected as MnNiSi, as it undergoes a structural transformation from hexagonal to orthorhombic at 1200 K upon cooling.[68,69] It was then tuned toward the HEA region with isostructural substitutions of Fe and Ge in appropriate amounts, formulating a RE-free quinary $Fe_{22.2}Ni_{22.2}Mn_{22.3}Ge_{16.65}Si_{16.65}$ HEA (its $\Delta S_{mix} = 1.60R$). Its temperature dependent synchrotron x-ray diffraction results show the phase transformation of hexagonal to orthorhombic structures, which is similar to that of MnNiSi.[6] In addition, its thermomagnetic curves also show abrupt changes in magnetization in the temperature regions that coincide with the temperatures at which synchrotron x-ray diffraction indicates that there is coexistence of both phases. This shows that the alloy undergoes a magnetostructural transformation in those temperature regions. A series of varying compositional ratio of Ge and Si in $Fe_{22.2}Ni_{22.2}Mn_{22.3}Ge_xSi_y$ HEAs, while adhering to the third criterion of the directed search approach, shows that the magnetostructural transformation temperatures can be further tuned to higher temperatures,[7] as shown in Fig. 8. Magnetostructural transformation of the alloys is observed for both virgin and repeated measurements, as displayed in Figs. 8(a) and 8(b), respectively. For both figures, abrupt changes in the magnetization with temperature are observed at the low temperature tails for all the alloys, which correspond to the magnetostructural transformation. The gradual change in magnetization with temperature at the higher temperature tails of the curves corresponds to the Curie transition of the higher temperature phase (hexagonal structure). These results also illustrate the efficiency and effectiveness to optimize HEAs in the vast compositional space once the starting HEA with the desired behavior is identified via a directed search strategy.

Furthermore, both $Fe_{22.2}Ni_{22.2}Mn_{22.3}Ge_{16.65}Si_{16.65}$ and $Fe_{22.2}Ni_{22.2}Mn_{22.3}Ge_{15.82}Si_{17.48}$ exhibit larger effective anisotropy fields at low temperatures (orthorhombic phase), which decrease at higher temperatures (hexagonal phase). This leads to the different thermomagnetic behavior for low and high magnetic fields [see the blue and red thermomagnetic curves in Fig. 9(a)]. As a result, inverse MCE (positive $\Delta S_{isothermal}$) is observed for low fields in Fig. 9(b) due to the increase in magnetization with temperature, while direct MCE (negative $\Delta S_{isothermal}$) is found for higher fields. In the repeated thermomagnetic measurements of $Fe_{22.2}Ni_{22.2}Mn_{22.3}Ge_{14.95}Si_{18.35}$, the abrupt increase in magnetization was not observed; thus, only the direct MCE is obtained. The authors have reported that the largest $\left|\Delta S^{peak}_{isothermal}\right|$ observed for the alloy with the highest Si content among this series was attributed to the vicinity of the magnetostructural transformation temperature and T_C of the high temperature hexagonal phase (refer to Ref. 6 for more details).

When comparing the MCE performance of the reported magnetocaloric HEAs in Fig. 10, Fe–Ni–Mn–Ge–Si HEAs exhibit the most promising MCE among others, in particular to their $\left|\Delta S^{peak}_{isothermal}\right|$ and $TEC(10)$ values. They show a significant improvement in the MCE performance, as high as an order of magnitude enhancement, among the RE-free magnetocaloric HEAs. This also indicates the independency of the large magnetic moments from RE

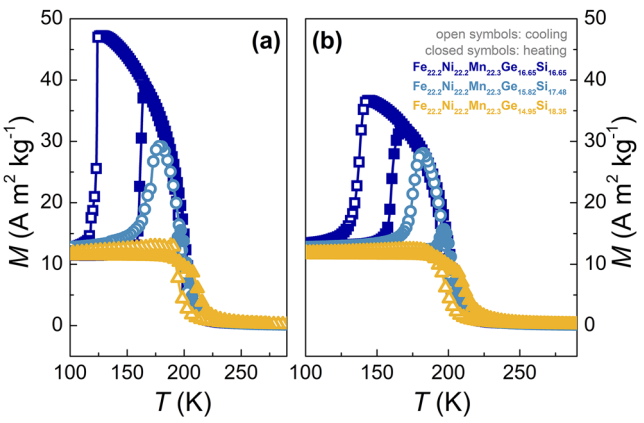

FIG. 8. Thermomagnetic curves of the RE-free Fe–Mn–Ni–Ge–Si HEAs measured at 2 K min^{-1} for 0.05 T: (a) virgin curves and (b) repeated measurements.

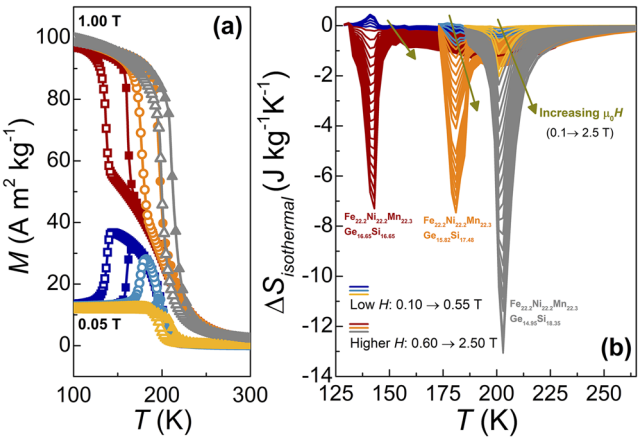

FIG. 9. (a) Low- and high-magnetic field thermomagnetic curves of RE-free Fe–Mn–Ni–Ge–Si HEAs measured at 2 K min^{-1}. (b) Isothermal entropy curves of the studied series measured up to 2.5 T using the discontinuous protocol. Closed and open symbols in (a) represent the data measured while heating and cooling, respectively.

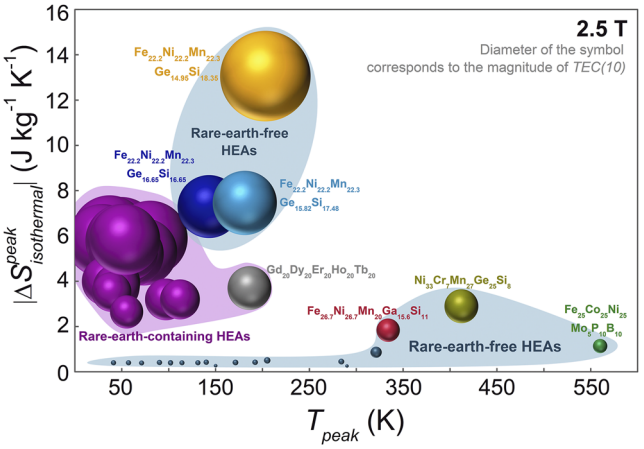

FIG. 10. MCE performance comparison of magnetocaloric HEAs for 2.5 T. Literature data collected from Refs. 6, 7, 13–16, 18, 19, 23, 29–32, 42, 43, 52, 53, 55, 57, and 58. Each data point represents a single material with a diameter proportional to its *TEC*(10).

elements. As seen in Fig. 7, Fe–Mn–Ni–Ge–Si HEAs close the pre-existing gap between notable magnetocaloric materials and the magnetocaloric HEAs prior to their reports. This points out that magnetostructural HEAs open a new path for the search of promising HEA magnetocaloric materials.

V. REQUIREMENTS FOR FUTURE MCE HEA

Nowadays, magnetocaloric materials suffer from several limitations when implemented into magnetic refrigeration devices, namely, poor mechanical stability, limited cyclic response, and thermal hysteresis. One of the aspects in which HEAs could contribute to the field of magnetic refrigeration is by enhancing mechanical properties. While in the case of single-phase solid solution HEAs, this comes without any additional effort,[22] the magnetic entropy change of these alloys is rather limited, putting them at the losing end when compared with high-performance conventional MCE materials. On the other hand, magnetostructural HEAs have significantly larger MCE but they still have lower mechanical performance than solid solution HEAs. One of the current goals in MCE-HEA research is to enhance the mechanical properties of these alloys while incorporating magnetostructural transformation. This would be achieved by processing and should not be considered an unreachable goal since shape memory alloys undergoing a martensitic transformation can have notable mechanical integrity upon cycling and even superplasticity. Detailed studies of the combined mechanical and functional performance of the alloys should be made in order to properly ascertain the improvement in applicability and reliability that these MCE-HEAs imply.

Thermal hysteresis can be addressed by compositional changes, tuning the temperature separation between the Curie and martensitic transitions. This is already evidenced in Fig. 9. Further substitutions should ameliorate the hysteresis of the transformation. The use of specific methodology such as Temperature First Order Reversal Curves (TFORCs)[70–72] would help in understanding the origin of hysteresis in these MCE-HEAs and facilitate their optimization.

For low-temperature applications, the dependence on heavy rare-earths should be reduced, probably by making hybrid RE-TM-HEAs. This broadens the search space much further, highlighting the importance of appropriate search strategies and high-throughput alloy synthesis and characterization.

VI. CONCLUSIONS AND PERSPECTIVES

Until recently, MCE-HEAs either were limited to low-temperature applications or had sub-par performance, making them less attractive than conventional materials. In the low temperature range, rare-earth HEAs have a relevant magnetocaloric performance. At higher temperatures, implementing a magnetostructural phase transition in rare-earth free HEAs boosts MCE response, increasing it by one order of magnitude.

The search inside the huge compositional space of HEAs has to be performed with a directed search strategy that takes the material from a low or medium-entropy alloy with the desired functionality toward the HEA space. Once HEAs with suitable functionality are found, their mechanical properties should be characterized and optimized via both compositional substitutions and processing techniques.

The implementation of HEAs with an optimal combination of functional and mechanical properties in devices and appliances will certainly improve their reliability and durability, increasing service life and leading us to a more sustainable economy.

SUPPLEMENTARY MATERIAL

The magnetocaloric properties discussed above, including other MCE figures of merit for 2 and 5 T, are provided in the supplementary material, in which the magnetocaloric HEAs are classified into RE-containing quinary (Table S1) and non-quinary (Table S2), and RE-free quinary (Table S3) and non-quinary (Table S4). In addition, their HEA empirical parameters are included.

ACKNOWLEDGMENTS

This work was supported by AEI/FEDER-UE (Grant No. PID2019-105720RB-I00), US/JUNTA/FEDER-UE (Grant No. US-1260179), Consejería de Economía, Conocimiento, Empresas y Universidad de la Junta de Andalucía (Grant No. P18-RT-746), and Army Research Laboratory under Cooperative Agreement No. W911NF-19-2-0212. J.Y.L. acknowledges a grant from VI Plan Propio de Investigación de la Universidad de Sevilla.

DATA AVAILABILITY

The data that support the findings of this study are available within the article and its supplementary material.

REFERENCES

[1]X. Wang, W. Guo, and Y. Fu, "High-entropy alloys: Emerging materials for advanced functional applications," J. Mater. Chem. A **9**, 663 (2021).

[2]M. C. Gao, J.-W. Yeh, P. K. Liaw, and Y. Zhang, *High Entropy Alloys: Fundamentals and Applications* (Springer International Publishing, Switzerland, 2016).
[3]Y.-F. Kao, S.-K. Chen, T.-J. Chen, P.-C. Chu, J.-W. Yeh, and S.-J. Lin, "Electrical, magnetic, and Hall properties of $Al_xCoCrFeNi$ high-entropy alloys," J. Alloys Compd. **509**, 1607 (2011).
[4]K. Zhang and Z. Fu, "Effects of annealing treatment on properties of $CoCrFeNiTiAl_x$ multi-component alloys," Intermetallics **28**, 34 (2012).
[5]V. Franco, J. S. Blázquez, J. J. Ipus, J. Y. Law, L. M. Moreno-Ramírez, and A. Conde, "Magnetocaloric effect: From materials research to refrigeration devices," Prog. Mater. Sci. **93**, 112 (2018).
[6]J. Y. Law, L. M. Moreno-Ramírez, Á. Díaz-García, A. Martín-Cid, S. Kobayashi, S. Kawaguchi, T. Nakamura, and V. Franco, "MnFeNiGeSi high-entropy alloy with large magnetocaloric effect," J. Alloys Compd. **855**, 157424 (2021).
[7]J. Y. Law, Á. Díaz-García, L. M. Moreno-Ramírez, and V. Franco, "Increased magnetocaloric response of FeMnNiGeSi high-entropy alloys," Acta Mater. **212**, 116931 (2021).
[8]E.-W. Huang, G.-Y. Hung, S. Y. Lee, J. Jain, K.-P. Chang, J. J. Chou, W.-C. Yang, and P. K. Liaw, "Mechanical and magnetic properties of the high-entropy alloys for combinatorial approaches," Crystals **10**, 200 (2020).
[9]K. Li and W. Chen, "Recent progress in high-entropy alloys for catalysts: Synthesis, applications, and prospects," Mater. Today Energy **20**, 100638 (2021).
[10]A. Perrin, D. E. Laughlin, and M. E. McHenry, "High entropy alloys: Magnetocaloric effects," in *Encyclopedia of Materials: Metals and Alloys* (Elsevier, 2021).
[11]H. Yin, J. Law, Y. Huang, V. Franco, H. Shen, S. Jiang, Y. Bao, and J. Sun, "Design of Fe-containing GdTbCoAl high-entropy-metallic-glass composite microwires with tunable Curie temperatures and enhanced cooling efficiency," Mater. Des. **206**, 109824 (2021).
[12]J. Y. Law and V. Franco, "Magnetocaloric composite materials," in *Encyclopedia of Materials: Composites*, edited by D. Brabazon (Elsevier, Oxford, 2021), Vol. 2, p. 461.
[13]M. S. Lucas, D. Belyea, C. Bauer, N. Bryant, E. Michel, Z. Turgut, S. O. Leontsev, J. Horwath, S. L. Semiatin, M. E. McHenry, and C. W. Miller, "Thermomagnetic analysis of $FeCoCr_xNi$ alloys: Magnetic entropy of high-entropy alloys," J. Appl. Phys. **113**, 17A923 (2013).
[14]D. D. Belyea, M. S. Lucas, E. Michel, J. Horwath, and C. W. Miller, "Tunable magnetocaloric effect in transition metal alloys," Sci. Rep. **5**, 15755 (2015).
[15]J. Huo, L. Huo, H. Men, X. Wang, A. Inoue, J. Wang, C. Chang, and R.-W. Li, "The magnetocaloric effect of Gd–Tb–Dy–Al–M (M = Fe, Co and Ni) high-entropy bulk metallic glasses," Intermetallics **58**, 31 (2015).
[16]L. Luo, H. Shen, Y. Bao, H. Yin, S. Jiang, Y. Huang, S. Guo, S. Gao, D. Xing, Z. Li, and J. Sun, "Magnetocaloric effect of melt-extracted high-entropy $Gd_{19}Tb_{19}Er_{18}Fe_{19}Al_{25}$ amorphous microwires," J. Magn. Magn. Mater. **507**, 166856 (2020).
[17]Z. Dong, Z. Wang, and S. Yin, "Magnetic properties and magneto-caloric effect (MCE) in $Cu_{22}Al_{18}Ho_{22}Tm_{20}Gd_{18}$ amorphous ribbons," J. Magn. Magn. Mater. **514**, 167270 (2020).
[18]Z. Dong, S. Huang, V. Ström, G. Chai, L. K. Varga, O. Eriksson, and L. Vitos, "$Mn_xCr_{0.3}Fe_{0.5}Co_{0.2}Ni_{0.5}Al_{0.3}$ high entropy alloys for magnetocaloric refrigeration near room temperature," J. Mater. Sci. Technol. **79**, 15 (2021).
[19]W. Sheng, J.-Q. Wang, G. Wang, J. Huo, X. Wang, and R.-W. Li, "Amorphous microwires of high entropy alloys with large magnetocaloric effect," Intermetallics **96**, 79 (2018).
[20]L. Li, C. Xu, Y. Yuan, and S. Zhou, "Large refrigerant capacity induced by table-like magnetocaloric effect in amorphous $Er_{0.2}Gd_{0.2}Ho_{0.2}Co_{0.2}Cu_{0.2}$ ribbons," Mater. Res. Lett. **6**, 413 (2018).
[21]A. Perrin, S. McCall, M. McElfresh, D. E. Laughlin, and M. E. McHenry, "Understanding magnetic exchange interactions by the pressure dependent Curie temperature in FeCoNiCuMn high entropy alloys," J. Phase Equilib. Diffus. (in press) (2021).
[22]Y. Zhang, T. T. Zuo, Z. Tang, M. C. Gao, K. A. Dahmen, P. K. Liaw, and Z. P. Lu, "Microstructures and properties of high-entropy alloys," Prog. Mater. Sci. **61**, 1 (2014).
[23]J. Huo, L. Huo, J. Li, H. Men, X. Wang, A. Inoue, C. Chang, J.-Q. Wang, and R.-W. Li, "High-entropy bulk metallic glasses as promising magnetic refrigerants," J. Appl. Phys. **117**, 073902 (2015).
[24]V. Franco and A. Conde, "Scaling laws for the magnetocaloric effect in second order phase transitions: From physics to applications for the characterization of materials," Int. J. Refrig. **33**, 465 (2010).
[25]Y. Zhang, B. Wu, D. Guo, J. Wang, and Z. Ren, "Magnetic properties and promising cryogenic magneto-caloric performances of $Gd_{20}Ho_{20}Tm_{20}Cu_{20}Ni_{20}$ amorphous ribbons," Chin. Phys. B **30**, 017501 (2021).
[26]Z. Dong, Z. Wang, and S. Yin, "Magnetic properties and large cryogenic magneto-caloric effect of $Er_{0.2}Tm_{0.2}Ho_{0.2}Cu_{0.2}Co_{0.2}$ amorphous ribbon," Intermetallics **124**, 106879 (2020).
[27]J. Li, L. Xue, W. Yang, C. Yuan, J. Huo, and B. Shen, "Distinct spin glass behavior and excellent magnetocaloric effect in $Er_{20}Dy_{20}Co_{20}Al_{20}RE_{20}$ (RE = Gd, Tb and Tm) high-entropy bulk metallic glasses," Intermetallics **96**, 90 (2018).
[28]M. Cai, Q. Luo, Q. Zeng, and B. Shen, "Combined effect of demagnetization field and magnetic anisotropy on magnetocaloric behavior and magnetocaloric-magnetoresistance correlation in GdTmErCoAl high-entropy amorphous alloy," J. Magn. Magn. Mater. **528**, 167817 (2021).
[29]L. Xue, L. Shao, Q. Luo, and B. Shen, "$Gd_{25}RE_{25}Co_{25}Al_{25}$ (RE = Tb, Dy and Ho) high-entropy glassy alloys with distinct spin-glass behavior and good magnetocaloric effect," J. Alloys Compd. **790**, 633 (2019).
[30]C. M. Pang, L. Chen, H. Xu, W. Guo, Z. W. Lv, J. T. Huo, M. J. Cai, B. L. Shen, X. L. Wang, and C. C. Yuan, "Effect of Dy, Ho, and Er substitution on the magnetocaloric properties of Gd–Co–Al–Y high entropy bulk metallic glasses," J. Alloys Compd. **827**, 154101 (2020).
[31]C. M. Pang, C. C. Yuan, L. Chen, H. Xu, K. Guo, J. C. He, Y. Li, M. S. Wei, X. M. Wang, J. T. Huo, and B. L. Shen, "Effect of Yttrium addition on magnetocaloric properties of Gd–Co–Al–Ho high entropy metallic glasses," J. Non-Cryst. Solids **549**, 120354 (2020).
[32]K. Wu, C. Liu, Q. Li, J. Huo, M. Li, C. Chang, and Y. Sun, "Magnetocaloric effect of $Fe_{25}Co_{25}Ni_{25}Mo_5P_{10}B_{10}$ high-entropy bulk metallic glass," J. Magn. Magn. Mater. **489**, 165404 (2019).
[33]J. Y. Law, R. V. Ramanujan, and V. Franco, "Tunable Curie temperatures in Gd alloyed Fe–B–Cr magnetocaloric materials," J. Alloys Compd. **508**, 14 (2010).
[34]X. C. Zhong, H. C. Tian, S. S. Wang, Z. W. Liu, Z. G. Zheng, and D. C. Zeng, "Thermal, magnetic and magnetocaloric properties of $Fe_{80-x}M_xB_{10}Zr_9Cu_1$ (M = Ni, Ta; x = 0, 3, 5) amorphous alloys," J. Alloys Compd. **633**, 188 (2015).
[35]J. Li, J. Y. Law, J. Huo, A. He, Q. Man, C. Chang, H. Men, J. Wang, X. Wang, and R.-W. Li, "Magnetocaloric effect of Fe–RE–B–Nb (RE = Tb, Ho or Tm) bulk metallic glasses with high glass-forming ability," J. Alloys Compd. **644**, 346 (2015).
[36]J. Li, J. Y. Law, H. Ma, A. He, Q. Man, H. Men, J. Huo, C. Chang, X. Wang, and R.-W. Li, "Magnetocaloric effect in Fe–Tm–B–Nb metallic glasses near room temperature," J. Non-Cryst. Solids **425**, 114 (2015).
[37]J. Li, J. Huo, J. Law, C. Chang, J. Du, Q. Man, X. Wang, and R.-W. Li, "Magnetocaloric effect in heavy rare-earth elements doped Fe-based bulk metallic glasses with tunable Curie temperature," J. Appl. Phys. **116**, 063902 (2014).
[38]W. Yang, J. Huo, H. Liu, J. Li, L. Song, Q. Li, L. Xue, B. Shen, and A. Inoue, "Extraordinary magnetocaloric effect of Fe-based bulk glassy rods by combining fluxing treatment and J-quenching technique," J. Alloys Compd. **684**, 29 (2016).
[39]H. Zhang, R. Li, T. Xu, F. Liu, and T. Zhang, "Near room-temperature magnetocaloric effect in FeMnPBC metallic glasses with tunable Curie temperature," J. Magn. Magn. Mater. **347**, 131 (2013).
[40]C. Liu, Q. Li, J. Huo, W. Yang, L. Chang, C. Chang, and Y. Sun, "Near room-temperature magnetocaloric effect of Co-based bulk metallic glass," J. Magn. Magn. Mater. **446**, 162 (2018).
[41]L. M. Moreno, J. S. Blázquez, J. J. Ipus, J. M. Borrego, V. Franco, and A. Conde, "Magnetocaloric effect of $Co_{62}Nb_6Zr_2B_{30}$ amorphous alloys obtained by mechanical alloying or rapid quenching," J. Appl. Phys. **115**, 17A302 (2014).
[42]J. Huo, J.-Q. Wang, and W.-H. Wang, "Denary high entropy metallic glass with large magnetocaloric effect," J. Alloys Compd. **776**, 202 (2019).
[43]Y. Yuan, Y. Wu, X. Tong, H. Zhang, H. Wang, X. J. Liu, L. Ma, H. L. Suo, and Z. P. Lu, "Rare-earth high-entropy alloys with giant magnetocaloric effect," Acta Mater. **125**, 481 (2017).

[44]V. Franco, "Determination of the magnetic entropy change from magnetic measurements: The importance of the measurement protocol," https://www.lakeshore.com/docs/default-source/software/vsm/mce-software/determination-of-the-magnetic-entropy-change-from-magnetic-measurements.pdf?sfvrsn=d14f68c1_2, 2014.
[45]J. Y. Law, V. Franco, L. M. Moreno-Ramírez, A. Conde, D. Y. Karpenkov, I. Radulov, K. P. Skokov, and O. Gutfleisch, "A quantitative criterion for determining the order of magnetic phase transitions using the magnetocaloric effect," Nat. Commun. **9**, 2680 (2018).
[46]S. F. Lu, L. Ma, G. H. Rao, J. Wang, Y. S. Du, L. Li, J. T. Zhao, X. C. Zhong, and Z. W. Liu, "Magnetocaloric effect of high-entropy rare-earth alloy GdTbHoErY," J. Mater. Sci.: Mater. Electron. **32**, 10919 (2021).
[47]S. F. Lu, L. Ma, J. Wang, Y. S. Du, L. Li, J. T. Zhao, and G. H. Rao, "Effect of configuration entropy on magnetocaloric effect of rare earth high-entropy alloy," J. Alloys Compd. **874**, 159918 (2021).
[48]J. Jensen and A. R. Mackintosh, *Rare Earth Magnetism: Structures and Excitations* (Clarendon Press, Oxford, 1991).
[49]M. S. Lucas, L. Mauger, J. A. Muñoz, Y. Xiao, A. O. Sheets, S. L. Semiatin, J. Horwath, and Z. Turgut, "Magnetic and vibrational properties of high-entropy alloys," J. Appl. Phys. **109**, 07E307 (2011).
[50]H. Ucar, J. J. Ipus, V. Franco, M. E. McHenry, and D. E. Laughlin, "Overview of amorphous and nanocrystalline magnetocaloric materials operating near room temperature," JOM **64**, 782 (2012).
[51]S.-M. Na, J.-H. Yoo, P. K. Lambert, and N. J. Jones, "Room-temperature ferromagnetic transitions and the temperature dependence of magnetic behaviors in FeCoNiCr-based high-entropy alloys," AIP Adv. **8**, 056412 (2018).
[52]S.-M. Na, P. K. Lambert, H. Kim, J. Paglione, and N. J. Jones, "Thermomagnetic properties and magnetocaloric effect of FeCoNiCrAl-type high-entropy alloys," AIP Adv. **9**, 035010 (2019).
[53]A. Quintana-Nedelcos, Z. Leong, and N. A. Morley, "Study of dual-phase functionalisation of NiCoFeCr–Al_x multicomponent alloys for the enhancement of magnetic properties and magneto-caloric effect," Mater. Today Energy **20**, 100621 (2021).
[54]Á. Díaz-García, J. Y. Law, P. Gębara, and V. Franco, "Phase deconvolution of multiphasic materials by the universal scaling of the magnetocaloric effect," JOM **72**, 2845 (2020).
[55]M. Kurniawan, A. Perrin, P. Xu, V. Keylin, and M. McHenry, "Curie temperature engineering in high entropy alloys for magnetocaloric applications," IEEE Magn. Lett. **7**, 6105005 (2016).
[56]S. Vorobiov, O. Pylypenko, Y. Bereznyak, I. Pazukha, E. Čižmár, M. Orendáč, and V. Komanicky, "Magnetic properties, magnetoresistive, and magnetocaloric effects of AlCrFeCoNiCu thin-film high-entropy alloys prepared by the co-evaporation technique," Appl. Phys. A **127**, 179 (2021).
[57]K. Sarlar, A. Tekgül, and I. Kucuk, "Magnetocaloric properties in a FeNiGaMnSi high entropy alloy," Curr. Appl. Phys. **20**, 18 (2020).
[58]K. Sarlar, A. Tekgul, and I. Kucuk, "Magnetocaloric properties of rare-earth-free $Mn_{27}Cr_7Ni_{33}Ge_{25}Si_8$ high-entropy alloy," IEEE Magn. Lett. **10**, 2109905 (2019).
[59]A. Perrin, M. Sorescu, V. Ravi, D. E. Laughlin, and M. E. McHenry, "Mössbauer analysis of compositional tuning of magnetic exchange interactions in high entropy alloys," AIP Adv. **9**, 035329 (2019).
[60]D. B. Miracle and O. N. Senkov, "A critical review of high entropy alloys and related concepts," Acta Mater. **122**, 448 (2017).
[61]B. E. MacDonald, Z. Fu, B. Zheng, W. Chen, Y. Lin, F. Chen, L. Zhang, J. Ivanisenko, Y. Zhou, H. Hahn, and E. J. Lavernia, "Recent progress in high entropy alloy research," JOM **69**, 2024 (2017).
[62]Y. Zhang, "Review of the structural, magnetic and magnetocaloric properties in ternary rare earth RE_2T_2X type intermetallic compounds," J. Alloys Compd. **787**, 1173 (2019).
[63]T.-L. Phan, T. A. Ho, T. V. Manh, N. T. Dang, C. U. Jung, B. W. Lee, and T. D. Thanh, "Y-doped $La_{0.7}Ca_{0.3}MnO_3$ manganites exhibiting a large magnetocaloric effect and the crossover of first-order and second-order phase transitions," J. Appl. Phys. **118**, 143902 (2015).
[64]L. M. Moreno-Ramírez, C. Romero-Muñiz, J. Y. Law, V. Franco, A. Conde, I. A. Radulov, F. Maccari, K. P. Skokov, and O. Gutfleisch, "Tunable first order transition in La(Fe, Cr, Si)$_{13}$ compounds: Retaining magnetocaloric response despite a magnetic moment reduction," Acta Mater. **175**, 406 (2019).
[65]L. M. Moreno-Ramírez, C. Romero-Muñiz, J. Y. Law, V. Franco, A. Conde, I. A. Radulov, F. Maccari, K. P. Skokov, and O. Gutfleisch, "The role of Ni in modifying the order of the phase transition of La(Fe, Ni, Si)$_{13}$," Acta Mater. **160**, 137 (2018).
[66]B. Kaeswurm, V. Franco, K. P. Skokov, and O. Gutfleisch, "Assessment of the magnetocaloric effect in La, Pr(Fe, Si) under cycling," J. Magn. Magn. Mater. **406**, 259 (2016).
[67]J. Y. Law, Á. Díaz-García, L. M. Moreno-Ramírez, V. Franco, A. Conde, and A. K. Giri, "How concurrent thermomagnetic transitions can affect magnetocaloric effect: The $Ni_{49-x}Mn_{36+x}In_{15}$ Heusler alloy case," Acta Mater. **166**, 459 (2019).
[68]V. Johnson and C. G. Frederick, "Magnetic and crystallographic properties of ternary manganese silicides with ordered Co_2P structure," Phys. Status Solidi A **20**, 331 (1973).
[69]V. Johnson, "Diffusionless orthorhombic to hexagonal transitions in ternary silicides and germanides," Inorg. Chem. **14**, 1117 (1975).
[70]V. Franco, T. Gottschall, K. P. Skokov, and O. Gutfleisch, "First-order reversal curve (FORC) analysis of magnetocaloric Heusler-type alloys," IEEE Magn. Lett. **7**, 6602904 (2016).
[71]L. M. Moreno-Ramírez and V. Franco, "Setting the basis for the interpretation of temperature first order reversal curve (TFORC) distributions of magnetocaloric materials," Metals **10**, 1039 (2020).
[72]Á. Díaz-García, J. Y. Law, L. M. Moreno-Ramírez, A. K. Giri, and V. Franco, "Deconvolution of overlapping first and second order phase transitions in a NiMnIn Heusler alloy using the scaling laws of the magnetocaloric effect," J. Alloys Compd. **871**, 159621 (2021).